VLF Notes

Paul Nicholson

2018-04-02

Contents

1 Incident Field

A completely polarised plane wave having arbitrary polarisation is incident from bearing θ with elevation β, as shown in figure 1.1.

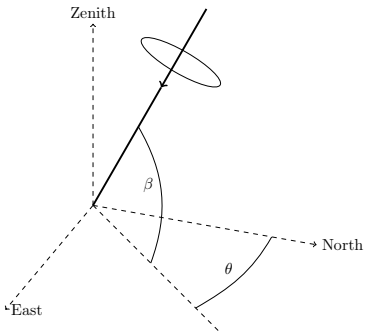

Figure 1.1: Signal incident on bearing θ with elevation β

The E-field can be represented as the sum of two perpendicular transverse components E_I and E_Q which are in phase quadrature. These components are related by

$$\begin{aligned} E_Q &= jPE_I \\ E_I &= \frac{1}{\sqrt{1+P^2}}E \\ E_Q &= \frac{jP}{\sqrt{1+P^2}}E \end{aligned} \tag{1.1}$$

where E is the complex incident E-field amplitude from which the real amplitude is given by $\Re(E\exp(j\omega t))$, and P is a polarisation parameter defined by

$$\begin{aligned} P = +1&\text{; right circular} \\ 0 < P < 1&\text{; right elliptical} \\ P = 0&\text{; linear polarisation} \\ 0 > P > -1&\text{; left elliptical} \\ P = -1&\text{; left circular} \end{aligned} \tag{1.2}$$

In these notes, the direction of rotation, left (anticlockwise) and right (clockwise), is defined looking along the wave vector towards the receiver. The locus of E traces out a polarisation ellipse in the plane of the wavefront, with orientation defined in figure 1.2a. E_I is positioned at a tilt angle α from the vertical plane of incidence. E_I and E_Q form the semi-major and semi-minor axes of the polarisation ellipse, and the ellipticity is given by $1/|P|$. Figure 1.2b shows the corresponding definitions of the H-field components.

The Stokes parameters are given in terms of the field strength and polarisation coefficient by

$$\begin{aligned} I &= E^2 \\ Q &= E^2\frac{P^2-1}{1+P^2}\cos 2\alpha \\ U &= E^2\frac{1-P^2}{1+P^2}\sin 2\alpha \\ V &= E^2\frac{2P}{1+P^2} \end{aligned} \tag{1.3}$$

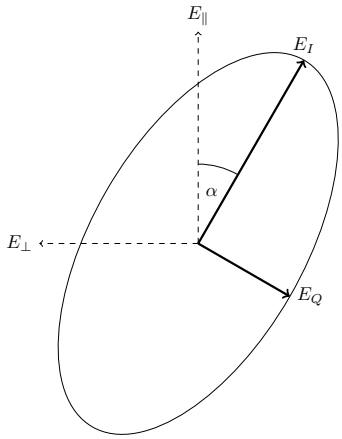

(a) E-field

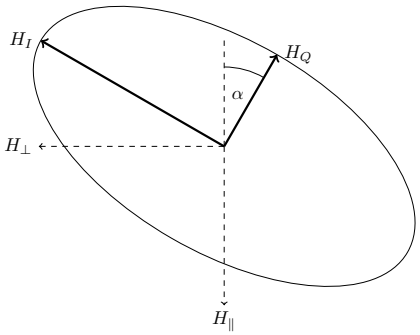

(b) H-field

Figure 1.2: Incident field in the plane of the wavefront, looking directly towards the wave normal. $E_\perp$ and $H_\parallel$ define the TE axes, $E_\parallel$ and $H_\perp$ define the TM axes.

Transverse components are resolved in the plane of the wavefront. TE components $E_\perp, H_\parallel$, and TM components $E_\parallel, H_\perp$ are resolved by

$$\begin{aligned} E_\perp &= -E_I\sin\alpha - E_Q\cos\alpha \\ E_\parallel &= E_I\cos\alpha - E_Q\sin\alpha \\ H_\perp &= H_I\cos\alpha - H_Q\sin\alpha \\ H_\parallel &= -H_I\sin\alpha - H_Q\cos\alpha \end{aligned} \tag{1.4}$$

2 Free-space Antenna Response

Vertical loop antennas will respond to the orthogonal horizontal components $H_\perp$ and $H_\parallel\sin\beta$ of the incident signal. A north/south aligned vertical loop antenna will experience a field strength of

$$H_{ns} = H_\perp\cos\theta - H_\parallel\sin\beta\sin\theta \tag{2.1}$$

which is the westward pointing component of the horizontal H-field. Similarly an east/west aligned loop will respond to the northward pointing component,

$$H_{ew} = H_\perp\sin\theta + H_\parallel\sin\beta\cos\theta \tag{2.2}$$

A vertical E-field probe responds to

$$E_v = E_\parallel\cos\beta \tag{2.3}$$

The loop orientations are shown in figure 2.1. Here the loop polarity is chosen such that a signal from the north-east will have H_{ns}, and H_{ew} both in phase with E_v.

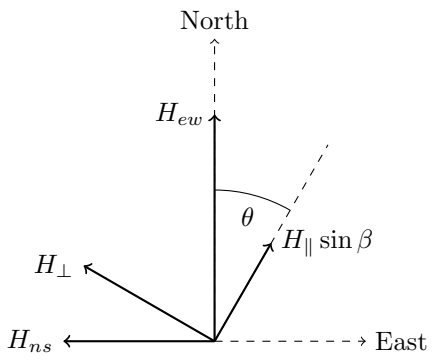

Figure 2.1: Plan view of the horizontal H-field components. The north pointing component H_{ew} is picked up by the east/west loop and the north/south loop responds to the west pointing component H_{ns}.

Substituting equations 1.1, 1.4 into 2.1 - 2.3 produces the orthogonal loop field strengths in terms of the incident field parameters,

$$\begin{aligned} H_{ns} &= H_I \{(\cos\alpha - jP\sin\alpha)\cos\theta \\ &\quad + (\sin\alpha + jP\cos\alpha)\sin\beta\sin\theta\} \\ H_{ew} &= H_I \{(\cos\alpha - jP\sin\alpha)\sin\theta \\ &\quad - (\sin\alpha + jP\cos\alpha)\sin\beta\cos\theta\} \\ E_v &= E_I(\cos\alpha - jP\sin\alpha)\cos\beta \end{aligned} \tag{2.4}$$

The presence of terms in jP ensures that for anything other than pure linear polarisation or a signal at zero elevation, the phase angle between the two loop signals will not be exactly 0 or π radians. Figure 2.2 shows the relative polarity of the received components in response to a signal from each quadrant.

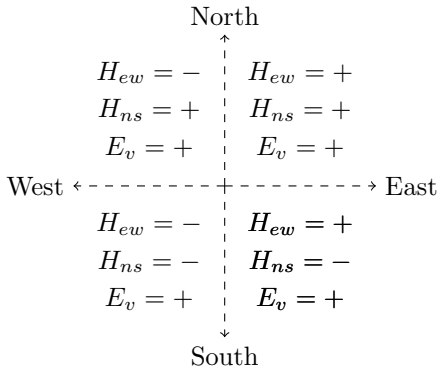

Figure 2.2: Relative polarity of the 3-axis received components.

3 Watson-Watt Goniometry

A loop at azimuth B will experience a field strength

$$H_B = H_{ns}\cos B + H_{ew}\sin B \tag{3.1}$$

An estimate $B = \hat{\theta}$ (modulo π) of the signal's azimuth is obtained when $|H_B|$ is at a maximum or minimum. This is determined by setting $d|H_B|/dB = 0$ which leads to

$$\begin{aligned} \hat{\theta} &= \frac{1}{2}\,\text{atan2}(H_{ew}H_{ns}^{\star} + H_{ew}^{\star}H_{ns}, |H_{ns}|^2 - |H_{ew}|^2) \\ &= \frac{1}{2}\,\text{atan2}(2|H_{ew}H_{ns}|\cos\delta, |H_{ns}|^2 - |H_{ew}|^2) \end{aligned} \tag{3.2}$$

where δ is the phase angle between the two loop signals. This corresponds to orientation of the major axis of the Lissajous ellipse formed on the Watson-Watt DF display.

Substituting from 2.4, the measured bearing in terms of the signal's true azimuth θ is given by

$$\hat{\theta} = \theta + \text{atan2}(F, G)/2 \tag{3.3}$$

where

$$\begin{aligned} F &= \sin(2\alpha)\sin\beta\left(P^2 - 1\right) \\ G &= \left(\sin^2\alpha - \cos^2\alpha\sin^2\beta\right)P^2 \\ &\quad - \sin^2\alpha\sin^2\beta + \cos^2\alpha \end{aligned} \tag{3.4}$$

The term atan2$(F, G)/2$ is referred to as the polarisation error. The error is zero when $F = 0$, therefore the error tends to zero with low elevation signals, with circular polarised signals, and with linear or elliptical polarisation where the major axis is vertical ($\alpha = 0$) or horizontal ($\alpha = \pi/2$).

The vertical E-field E_v can be used to resolve the ambiguity of π radians inherent in equation 3.2. First, the signal from a loop aligned on $\hat{\theta}$ is constructed,

$$H_b = H_{ns}\cos\hat{\theta} + H_{ew}\sin\hat{\theta} \tag{3.5}$$

The cosine of the phase angle between H_b and E_v is then examined and if negative, π radians is added to $\hat{\theta}$

4 Poynting Vector Method

In section 3 the E-field component was used only to resolve the π radian ambiguity of the bearing derived from the orthogonal loops. This does not use all the information available from the phase of the E_v component and a better estimate is obtained with the following,

$$\begin{aligned} \hat{\theta} &= \arctan\left(\frac{|H_{ew}E_v^{\star}|\cos\delta_1}{|H_{ns}E_v^{\star}|\cos\delta_2}\right) \\ &= \arctan\left(\frac{H_{ew}E_v^{\star} + H_{ew}^{\star}E_v}{H_{ns}E_v^{\star} + H_{ns}^{\star}E_v}\right) \end{aligned} \tag{4.1}$$

where δ_1 and δ_2 are the phase differences between H_{ew} and E_v, and between H_{ns} and E_v, respectively. Equation 4.1 is derived by considering the horizontal components of the Poynting vector and discarding the products of horizontal electric field and vertical magnetic field. As before, substituting from 2.4 gives the measured bearing in terms of the signal's true azimuth plus a polarisation error term,

$$\hat{\theta} = \theta + \arctan\left(\frac{\cos\alpha\sin\alpha\sin\beta(P^2 - 1)}{\cos^2\alpha + P^2\sin^2\alpha}\right) \tag{4.2}$$

The polarisation error with this method is always less than or equal to the goniometric polarisation error, and in many cases is much less. In particular the error is zero for horizontal or vertical linear polarisation, and for both states of pure circular polarisation.

5 Tsuruda and Hayashi NPE method

If the incident signal is not linearly polarised (at VLF, signals almost never have linear polarisation), then there will be some phase difference between the three measured components. Let $\delta_1, \delta_2, \delta_3$ be the phase differences, defined by

$$\begin{aligned} \delta_1 &= \arg(E_v/H_{ew}) \\ \delta_2 &= \arg(E_v/H_{ns}) \\ \delta_3 &= \arg(H_{ns}/H_{ew}) \end{aligned} \tag{5.1}$$

The sines of these angles are given by the identities

$$\begin{aligned} \sin\delta_1 &= j(E_v H_{ew}^\star - E_v^\star H_{ew})/(2|E_v||H_{ew}|) \\ \sin\delta_2 &= j(E_v H_{ns}^\star - E_v^\star H_{ns})/(2|E_v||H_{ns}|) \\ \sin\delta_3 &= j(H_{ns} H_{ew}^\star - H_{ns}^\star H_{ew})/(2|H_{ns}||H_{ew}|) \end{aligned} \tag{5.2}$$

Eliminating terms involving α and P from equations 2.4 gives

$$E_v = E_I(H_{ew}\sin\theta + H_{ns}\cos\theta)\cos\beta \tag{5.3}$$

Using 5.3 to eliminate E_v from 5.2 leads to an expression for θ

$$\theta = -\arctan\left(\frac{|H_{ns}|\sin\delta_2/\sin\delta_3}{|H_{ew}|\sin\delta_1/\sin\delta_3}\right) \tag{5.4}$$

in which the atan2() function should be used in order to preserve quadrant information. This is an exact expression for θ and therefore there is no polarisation error (NPE). This method relies on accurate determination of the phase angles between the three components.

6 Angle Averaging

It is often necessary to produce an average of several azimuth or phase angle measurements. However the normal arithmetic mean of the angles fails, since for example mean(20 + 40) = 30 works fine, but mean(350 + 30) = 190 fails. Any particular case can be dealt with by a repositioning of the angle meridian or by addition or substraction of whole cycles. For example in this case mean(−10 + 30) = 10, and this leads to the Mitsuta algorithm.

An alternative method which performs better when the raw angles are very noisy involves summing the direction cosines. Given a set θ_i of raw angles in radians, the direction cosines are summed and the average angle is produced by the atan2() function,

$$A = \sum_{i=1}^{N}\sin\theta_i \quad ; \quad B = \sum_{i=1}^{N}\cos\theta_i \tag{6.1}$$

$$\text{average} = \text{atan2}(A, B) \tag{6.2}$$

The above is conveniently carried out using complex arithmetic,

$$\text{average} = \arg\left(\sum_{i=1}^{N}(\cos\theta_i + j\sin\theta_i)\right) \tag{6.3}$$

```
sum = D = b[1];
sumsq = D * D;

for( i from 2 to N)
{
   delta = b[i] - D;

   if( delta < -180) D = D + delta + 360;
   else
   if( delta < 180) D = D + delta;
   else
      D = D + delta - 360;

   sum = sum + D;
   sumsq = sumsq + D * D;
}

mean = sum/N;
std_dev = sqrt(sumsq/N - mean * mean);
```

Listing 6.1: Mitsuta algorithm operating on an array $b[1..N]$ of raw bearings mod 360. For mod 180 operation, replace 360 and 180 by 180 and 90.

It is usually desirable to weight each contribution to the average, eg by the signal power or amplitude. If each θ_i has weight w_i, then

$$\text{average} = \arg\left(\sum_{i=1}^{N} w_i(\cos\theta_i + j\sin\theta_i)\right) \tag{6.4}$$

If the angles are modulo π radians, then the averaging formula becomes

$$\text{average} = \frac{1}{2}\arg\left(\sum_{i=1}^{N} w_i(\cos 2\theta_i + j\sin 2\theta_i)\right) \tag{6.5}$$

The direction cosine averaging does not offer a standard deviation but an accurate approximation is obtained with the Yamartino formula,

$$S = \sum_{i=1}^{N} w_i(\cos\theta_i + j\sin\theta_i) \quad , \quad W = \sum_{i=1}^{N} w_i \tag{6.6}$$

$$\begin{aligned} \text{standard deviation} &\approx (1 + 0.1547x^3)\sin^{-1}x \\ \text{where} \quad x &= \sqrt{1 - |S|^2/W^2} \end{aligned} \tag{6.7}$$

7 Loop Alignment Correction

Signal analysis assumes the availability of orthogonal loop signals, eg H_{ew}, H_{ns}. In practice the actual loop signals may not be so aligned, or even orthogonal, due to site or installation limits, or distortion of the effective loop plane due to non-uniform ground properties or nearby structures. A linear transformation must be applied to the loop signals to synthesise the desired orthogonal loop signals.

Signals H_1 and H_2 from loops having effective azimuth A_1 and A_2 respectively, and $A_1 \neq A_2 \pmod\pi$, are given by

$$\begin{bmatrix} H_1 \\ H_2 \end{bmatrix} = \begin{bmatrix} \cos A_1 & \sin A_1 \\ \cos A_2 & \sin A_2 \end{bmatrix} \begin{bmatrix} H_{ns} \\ H_{ew} \end{bmatrix} \tag{7.1}$$

Inverting the above expression gives a formula by which H_{ns} and H_{ew} can be synthesised from the loop signals.

$$\begin{bmatrix} H_{ns} \\ H_{ew} \end{bmatrix} = \frac{1}{D} \begin{bmatrix} \sin A_2 & -\sin A_1 \\ -\cos A_2 & \cos A_1 \end{bmatrix} \begin{bmatrix} H_1 \\ H_2 \end{bmatrix} \tag{7.2}$$
$$D = \cos A_1 \sin A_2 - \sin A_1 \cos A_2$$

8 Ground Reflections

The VLF antenna is normally located much less than a wavelength above ground and therefore the loops and E-field probe will respond to the superposition of the incident field and the field resulting from ground reflection. This section deals with the ground reflection local to the antenna, in which the reflected signal has negligible propagation delay compared with the incident signal. Distant ground reflections produce multi-path signals which are considered in another section.

The ground is assumed to be isotropic and non-magnetic and described by the following physical attributes

Permeability μ_0

$$\text{Conductivity } \sigma_g = \begin{cases} 1 \times 10^{-3}\,\text{mhos/m} & \text{(poor ground)} \\ 5 \times 10^{-3}\,\text{mhos/m} & \text{(average ground)} \\ 2 \times 10^{-2}\,\text{mhos/m} & \text{(good ground)} \\ 5\,\text{mhos/m} & \text{(sea)} \end{cases}$$

$$\text{Permittivity } \epsilon_g = \begin{cases} 5\epsilon_0 & \text{(poor ground)} \\ 15\epsilon_0 & \text{(average ground)} \\ 25\epsilon_0 & \text{(good ground)} \\ 80\epsilon_0 & \text{(sea)} \end{cases}$$

and the following derived quantities

TM reflection coefficient	$\Gamma_\parallel(\beta)$
TE reflection coefficient	$\Gamma_\perp(\beta)$
Complex refractive index	$\tilde{n} = \sqrt{(\epsilon_g - j\sigma_g/\omega)/\epsilon_0}$

The reflection coefficients are functions of the elevation angle β of the incident field described in section 1. Isotropic ground implies the reflected and incident wave normals share the same plane of incidence with azimuth θ. Lossy conductive ground produces a complex refractive index $\tilde{n}$.

Isotropic ground implies that TM and TE components are uncoupled and reflected independently, so they can be analysed separately. Separating the field into TM and TE components, and separating each of these into incident and reflected, perpendicular and parallel H and E field strengths, we have

$$\begin{aligned} E_\parallel^\triangledown &= \text{incident parallel E-field} \\ H_\perp^\triangledown &= \text{incident perpendicular H-field} \\ E_\perp^\triangledown &= \text{incident perpendicular E-field} \\ H_\parallel^\triangledown &= \text{incident parallel H-field} \\ E_\parallel^\triangle &= \text{reflected parallel E-field} \\ H_\perp^\triangle &= \text{reflected perpendicular H-field} \\ E_\perp^\triangle &= \text{reflected perpendicular E-field} \\ H_\parallel^\triangle &= \text{reflected parallel H-field} \end{aligned} \tag{8.1}$$

The orientations of these components are defined in figure 8.1. The four components of the incident field are given by equation 1.4.

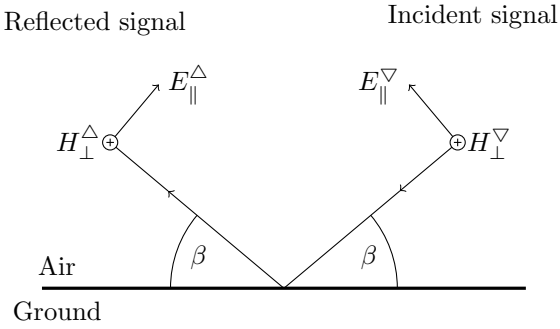

(a) TM components

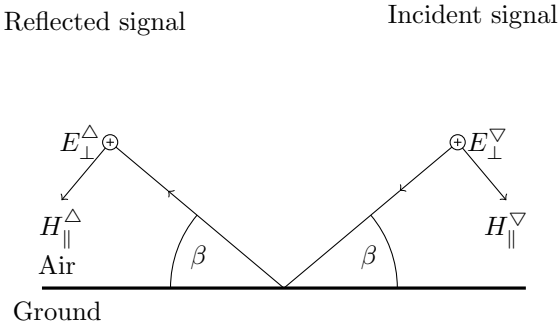

(b) TE components

Figure 8.1: Incident and reflected field components, in the plane of incidence

The following Fresnel reflection coefficients apply,

$$\begin{aligned} \Gamma_\parallel &= \frac{H_\perp^\triangle}{H_\perp^\triangledown} = \frac{\tilde{n}^2 \sin\beta - \sqrt{\tilde{n}^2 - \cos^2\beta}}{\tilde{n}^2 \sin\beta + \sqrt{\tilde{n}^2 - \cos^2\beta}} \\ \Gamma_\perp &= \frac{E_\perp^\triangle}{E_\perp^\triangledown} = \frac{\sin\beta - \sqrt{\tilde{n}^2 - \cos^2\beta}}{\sin\beta + \sqrt{\tilde{n}^2 - \cos^2\beta}} \end{aligned} \tag{8.2}$$

As ground conductivity improves, $\Gamma_\perp \to -1$ and $\Gamma_\parallel \to +1$. At VLF this is particularly so since $\sigma_g/\omega \gg \epsilon_g$ even with poor ground.

The horizontal E-field perpendicular to the plane of incidence is $-E_\perp^\triangledown - E_\perp^\triangle = -E_\perp^\triangledown(1+\Gamma_\perp)$. The horizontal radial E-field (pointing towards the source) is $-E_\perp^\triangledown(1-\Gamma_\parallel)\sin\beta$. Both these components tend to zero with typical VLF reflection coefficients. Table 8.1 shows some typical values

Freq	poor gnd	avg gnd	good gnd	sea
0.2kHz	0.99∠-0	1.00∠-0	1.00∠-0	1.00∠-0
1.0kHz	0.99∠-1	0.99∠-0	1.00∠-0	1.00∠-0
5.0kHz	0.97∠-2	0.99∠-1	0.99∠-0	1.00∠-0
20.0kHz	0.95∠-3	0.98∠-1	0.99∠-1	1.00∠-0
50.0kHz	0.92∠-5	0.96∠-2	0.98∠-1	1.00∠-0

(a) TM reflection coefficient $\Gamma_{\parallel}$, 60 deg elevation

Freq	poor gnd	avg gnd	good gnd	sea
0.2kHz	0.97∠-2	0.99∠-1	0.99∠-0	1.00∠-0
1.0kHz	0.94∠-3	0.97∠-2	0.99∠-1	1.00∠-0
5.0kHz	0.87∠-8	0.94∠-3	0.97∠-2	1.00∠-0
20.0kHz	0.76∠-16	0.89∠-7	0.94∠-3	1.00∠-0
50.0kHz	0.66∠-25	0.83∠-11	0.91∠-6	0.99∠-0

(b) TM reflection coefficient $\Gamma_{\parallel}$, 10 deg elevation

Freq	poor gnd	avg gnd	good gnd	sea
0.2kHz	-1.00∠-0	-1.00∠-0	-1.00∠-0	-1.00∠-0
1.0kHz	-0.99∠-1	-1.00∠-0	-1.00∠-0	-1.00∠-0
5.0kHz	-0.98∠-1	-0.99∠-1	-1.00∠-0	-1.00∠-0
20.0kHz	-0.96∠-2	-0.98∠-1	-0.99∠-1	-1.00∠-0
50.0kHz	-0.94∠-4	-0.97∠-2	-0.99∠-1	-1.00∠-0

(c) TE reflection coefficient $\Gamma_{\perp}$, 60 deg elevation

Freq	poor gnd	avg gnd	good gnd	sea
0.2kHz	-1.00∠-0	-1.00∠-0	-1.00∠-0	-1.00∠-0
1.0kHz	-1.00∠-0	-1.00∠-0	-1.00∠-0	-1.00∠-0
5.0kHz	-1.00∠-0	-1.00∠-0	-1.00∠-0	-1.00∠-0
20.0kHz	-0.99∠-0	-1.00∠-0	-1.00∠-0	-1.00∠-0
50.0kHz	-0.99∠-1	-0.99∠-0	-1.00∠-0	-1.00∠-0

(d) TE reflection coefficient $\Gamma_{\perp}$, 10 deg elevation

Table 8.1: Reflection coefficients for various grounds with low and high elevation signals. Phase angles are in degrees.

for $\Gamma_{\parallel}$ and $\Gamma_{\perp}$ for various types of ground. The TM reflection coefficient exhibits a clear Brewster effect at very low elevation. This is illustrated in figure 8.2. The reflection coefficient is a minimum at the Brewster angle and below this angle the phase of the reflection is reversed. The Brewster angle increases as the frequency or ground resistance increases.

9 Antenna Response With Ground Reflection

The components of the superposition of the incident and reflected fields relevant for 3-axis reception, as defined in section 2, are

$$\begin{aligned} H_{ns} &= -H_{\parallel}^{\triangledown}(1-\Gamma_{\perp})\sin\beta\sin\theta + H_{\perp}^{\triangledown}(1+\Gamma_{\parallel})\cos\theta \\ H_{ew} &= H_{\parallel}^{\triangledown}(1-\Gamma_{\perp})\sin\beta\cos\theta + H_{\perp}^{\triangledown}(1+\Gamma_{\parallel})\sin\theta \\ E_v &= E_{\parallel}^{\triangledown}(1+\Gamma_{\parallel})\cos\beta \end{aligned} \tag{9.1}$$

The horizontal components are illustrated in figure 9.1. Substituting the definitions of the incident field from equations 1.1, 1.4 leads to

(9.2)

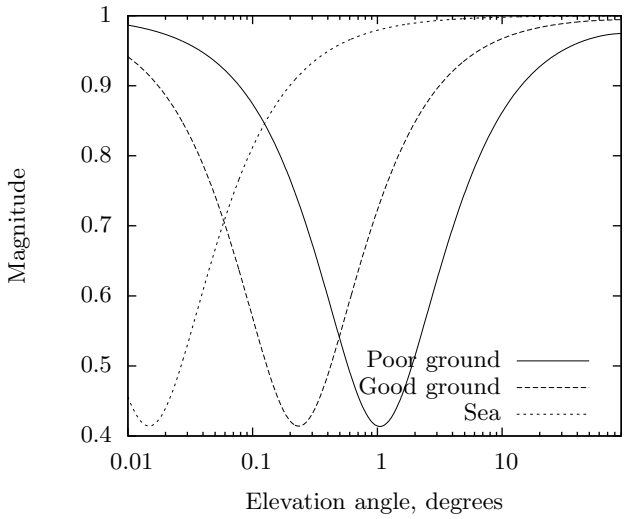

(a) Magnitude

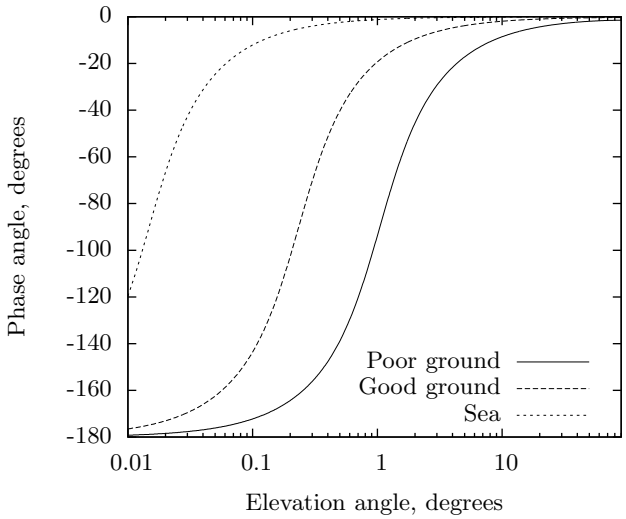

(b) Phase

Figure 8.2: Ground reflection coefficient $\Gamma_{\parallel}$ at 6kHz as a function of elevation.

$$\begin{aligned} H_{ns} &= H_I\left\{(1+\Gamma_{\parallel})(\cos\alpha - jP\sin\alpha)\cos\theta\right. \\ &\qquad \left. + (1-\Gamma_{\perp})(\sin\alpha + jP\cos\alpha)\sin\beta\sin\theta\right\} \\ H_{ew} &= H_I\left\{(1+\Gamma_{\parallel})(\cos\alpha - jP\sin\alpha)\sin\theta\right. \\ &\qquad \left. - (1-\Gamma_{\perp})(\sin\alpha + jP\cos\alpha)\sin\beta\cos\theta\right\} \\ E_v &= E_I(1+\Gamma_{\parallel})(\cos\alpha - jP\sin\alpha)\cos\beta \end{aligned} \tag{9.3}$$

In the absence of any ground reflection, $\Gamma_{\parallel} = \Gamma_{\perp} = 0$ and 9.3 reduces to 2.4.

10 Elevation Estimation

Consider a vertical loop in the plane of incidence, azimuth θ. This will respond to a horizontal magnetic field component of

$$\begin{aligned} H(\theta) &= H_{\perp}^{\triangledown} + H_{\perp}^{\triangle} \\ &= H_I(1+\Gamma_{\parallel})(\cos\alpha - jP\sin\alpha) \\ &= H_{ew}\sin\theta + H_{ns}\cos\theta \end{aligned} \tag{10.1}$$

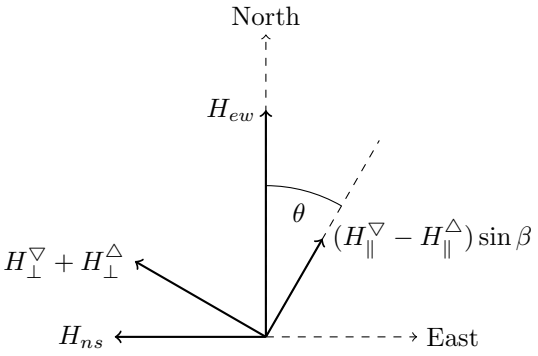

Figure 9.1: Plan view of the horizontal H-field components. The north pointing component H_{ew} is picked up by the east/west loop and the north/south loop responds to the west pointing component H_{ns}.

Then from equation 9.3, it is clear that E_v and H_b are in phase irrespective of ground reflection and signal polarisation, and

$$\frac{E_v}{H(\theta)} = \frac{E_I}{H_I}\cos\beta = Z_0\cos\beta \tag{10.2}$$

where Z_0 is the free space impedance.

If an estimate $\hat{\theta}$ of the signal azimuth is obtained using one of the direction finding methods described earlier, then an elevation estimate $\hat{\beta}$ is given by

$$\hat{\beta} = \cos^{-1}\left\{\frac{E_v/Z_0}{H_{ew}\sin\hat{\theta} + H_{ns}\cos\hat{\theta}}\right\} \tag{10.3}$$

When $\hat{\theta}$ is obtained by goniometry or Poynting vector methods, the resulting $\hat{\beta}$ can have large error, especially for signals with nearly linear and horizontal polarisation.

11 Polarisation Estimation

Once the signal azimuth and elevation are measured using the methods described earlier, the signal polarisation P and tilt angle α can be determined.

A vertical loop in the plane of incidence intercepts a field component

$$\begin{aligned} H(\theta) &= H_{\perp}^{\triangledown} + H_{\perp}^{\triangle} \\ &= H_I(1+\Gamma_{\parallel})(\cos\alpha - jP\sin\alpha) \end{aligned} \tag{11.1}$$

and this signal is synthesised from the H_{ew} and H_{ns} loop signals with

$$H(\theta) = H_{ew}\sin\theta + H_{ns}\cos\theta \tag{11.2}$$

Similarly, a loop oriented perpendicular (rotated clockwise) to the plane of incidence intercepts a field component

$$\begin{aligned} H(\theta+\pi/2) &= \left(H_{\parallel}^{\triangledown} - H_{\parallel}^{\triangle}\right)\sin\beta \\ &= -H_I(1-\Gamma_{\perp})(\sin\alpha + jP\cos\alpha)\sin\beta \end{aligned} \tag{11.3}$$

which is synthesised with

$$H(\theta+\pi/2) = H_{ew}\cos\theta - H_{ns}\sin\theta \tag{11.4}$$

Orthogonal components of the incident field in the plane of the polarisation ellipse, $H_{\perp}$ and $H_{\parallel}$, as defined in figure 1.2b and equation 1.4 are then obtained by correcting for the ground reflection and signal elevation,

$$\begin{aligned} H_{\perp} &= \frac{H(\theta)}{(1+\Gamma_{\parallel})} \\ H_{\parallel} &= \frac{H(\theta+\pi/2)}{(1-\Gamma_{\perp})\sin\beta} \end{aligned} \tag{11.5}$$

The tilt angle α is then given by

$$\begin{aligned} \delta &= \arg(H_{\parallel}/H_{\perp}) \\ \alpha &= -\frac{1}{2}\tan^{-1}\left(\frac{2|H_{\parallel}||H_{\perp}|\cos(\delta)}{|H_{\parallel}|^2 - |H_{\perp}|^2}\right) \\ &= -\frac{1}{2}\tan^{-1}\left(\frac{H_{\parallel}H_{\perp}^{\star} + H_{\parallel}^{\star}H_{\perp}}{H_{\parallel}H_{\parallel}^{\star} - H_{\perp}H_{\perp}^{\star}}\right) \end{aligned} \tag{11.6}$$

which should be implemented with the atan2() function. Then the polarisation parameter P is given by

$$P = -j\frac{H_{\perp}\sin\alpha + H_{\parallel}\cos\alpha}{H_{\parallel}\sin\alpha - H_{\perp}\cos\alpha} \tag{11.7}$$

In practice, the values of azimuth and elevation used in these formulas are the estimates $\hat{\theta}, \hat{\alpha}$ obtained through one of the methods described earlier. If $\hat{\theta}$ is obtained by goniometry, then $H(\hat{\theta})$ and $H(\hat{\theta}+\pi/2)$ are in exact phase quadrature and the resulting α is zero, with $\mathrm{sgn}(P) = -\mathrm{sgn}(\arg(H(\hat{\theta}+\pi/2)/H(\hat{\theta})))$.

12 Ionospheric Reflection

The D-layer can be approximated by a smooth sharp boundary above which is a cold neutral plasma with the following physical characteristics.

$$\begin{aligned} \omega_g &= B_M q_e/m_e = \text{electron gyro frequency} \\ \omega_p &= q_e\sqrt{\frac{N_e}{\epsilon_0 m_e}} = \text{electron plasma frequency} \\ \nu &= \text{electron collision frequency} \\ m_e &= \text{electron mass,} 9.109\times10^{-31} Kg \\ N_e &= \text{electron density} \\ q_e &= \text{electron charge,} 1.602\times10^{-19} \quad \text{Coulombs} \\ B_M &= \text{static field flux density} \approx 50\text{uT} \\ \epsilon_0 &= 8.854\times10^{-12} \end{aligned} \tag{12.1}$$

The electron density N_e varies with solar zenith angle and increases exponentially with height. Estimates can be obtained from the IRI model. Figure 12.1 shows some typical mid-latitude values. The electron-neutral collision frequency ν is a function of density and temperature. A useful approximation as a function of height, based on observational results (Wait & Spies 1964) is given by

$$\nu(h) = 1.816\times10^{11}\exp\left(-1.5\times10^{-4}h\right) \tag{12.2}$$

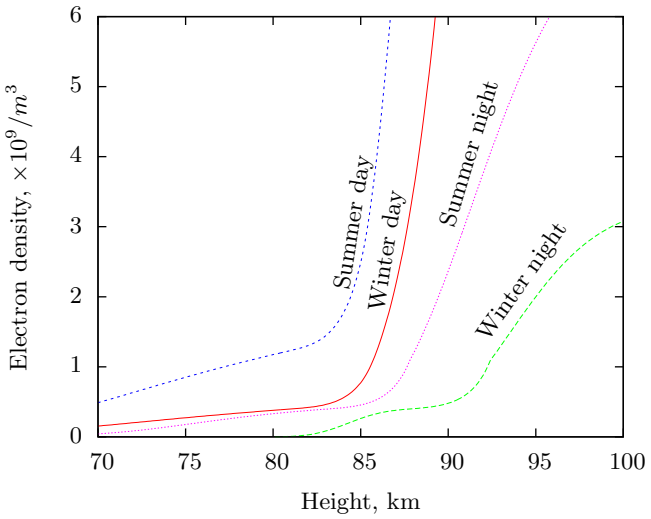

Figure 12.1: Electron density in the D-layer, calculated for western Europe using the IRI model.

In terms of these plasma properties, the reflection coefficients are

$$
\begin{aligned}
{}_{\parallel}\Gamma_{\parallel} &= (E+F)/D \\
{}_{\parallel}\Gamma_{\perp} &= 2jC(\tilde{n}_o C_o - \tilde{n}_e Ce)/D \\
{}_{\perp}\Gamma_{\parallel} &= 2jC(\tilde{n}_o C_e - \tilde{n}_e Co)/D \\
{}_{\perp}\Gamma_{\perp} &= (E-F)/D \\
C &= \cos\phi \\
C_o &= \cos\phi_o \\
C_e &= \cos\phi_e \\
D &= (\tilde{n}_o + \tilde{n}_e)(C^2 + C_o C_e) \\
&\quad + (\tilde{n}_o\tilde{n}_e + 1)(C_o + C_e)C \\
E &= (\tilde{n}_o + \tilde{n}_e)(C^2 - C_o C_e) \\
F &= (\tilde{n}_o\tilde{n}_e - 1)(C_o + C_e)C \\
\phi_o &= \sin^{-1}\frac{\sin\phi}{\tilde{n}_o} \\
\phi_e &= \sin^{-1}\frac{\sin\phi}{\tilde{n}_e}
\end{aligned}
\tag{12.3}
$$

The two complex refractive indices $\tilde{n}_o$ and $\tilde{n}_e$ determine the propagation. An arbitrary wave is decomposed into components parallel and perpendicular to the static magnetic field. For the perpendicular component, $\tilde{n}_o$ applies to the ordinary wave and $\tilde{n}_e$ to the extraordinary wave. For the parallel component, the $\tilde{n}_o$ and $\tilde{n}_e$ describe opposite states of circular polarisation.

The values of $\tilde{n}_o$ and $\tilde{n}_e$ are obtained from the Appleton-Hartree equations,

Property	Day	Night
Effective height, h	70×10^3	90×10^3
Electron density, N_e	3×10^8	1×10^6

Table 12.1: Typical values of D-layer physical properties

$$
\begin{aligned}
\tilde{n}_o^2 &= 1 - \frac{X}{A_1 + \frac{A_2}{1-X-iZ}} \\
\tilde{n}_e^2 &= 1 - \frac{X}{A_1 - \frac{A_2}{1-X-iZ}}
\end{aligned}
$$

where

$$
\begin{aligned}
A_1 &= 1 - iZ - \frac{\frac{1}{2}Y^2\sin^2\theta_m}{1-X-iZ} \\
A_2 &= \left(\frac{1}{4}Y^4\sin^4\theta_m + Y^2\cos^2\theta_m\,(1-X-iZ)^2\right)^{1/2} \\
X &= \omega_p^2/\omega^2 \\
Y &= \omega_g/\omega \\
Z &= \nu/\omega \\
\theta_m &= \text{angle between wave direction and magnetic field}
\end{aligned}
\tag{12.4}
$$

At VLF, $\nu \ll \omega$ and therefore Z is usually approximated by zero, thus treating the plasma as collisionless.

At VLF and at mid to high latitudes, it is common to invoke the quasi-linear (QL) approximation in which only the vertical component of the static magnetic field is considered. This produces reflection coefficients which are independent of the angle of incidence to the magnetic field and therefore there is no difference between eastwards and westwards propagation. With the QL approximation the refractive indices simplify to

$$
\begin{aligned}
\tilde{n}_o &= \sqrt{1 - j(\omega_\tau/\omega)e^{+j\tau}} \\
\tilde{n}_e &= \sqrt{1 - j(\omega_\tau/\omega)e^{-j\tau}} \\
\tau &= \tan^{-1}(\omega_g/\nu) \\
\omega_\tau &= \omega_p^2\sqrt{\nu^2 + \omega_g^2}
\end{aligned}
\tag{12.5}
$$

Anisotropy due to the static magnetic field produces coupling between TM and TE modes during reflection. Four complex amplitude reflection coefficients are therefore required. These are

$$
\begin{aligned}
{}_{\parallel}\Gamma_{\parallel} &= \text{TM to TM} \\
{}_{\parallel}\Gamma_{\perp} &= \text{TM to TE} \\
{}_{\perp}\Gamma_{\perp} &= \text{TE to TE} \\
{}_{\perp}\Gamma_{\parallel} &= \text{TE to TM}
\end{aligned}
\tag{12.6}
$$

The values of these coefficients depend on the zenith angle of incidence ϕ and the angle θ_m between the incident signal and the static magnetic field.

13 Convergence/Divergence Factor

Signals incident on the ionosphere from below encounter a concave reflector and therefore experience a focusing effect on reflection. Conversely, the ground is a convex reflector and produces a divergence of reflected rays. These factors are quite significant and are accounted for by a convergence coefficient.

$$\begin{aligned}
\alpha(n) &= (1 + h/R_E)\sqrt{\alpha_1(n)\alpha_2(n)} \\
\alpha_1(n) &= \frac{2n \sin\xi}{\sin\left(\frac{d}{R_E}\right)} \\
\alpha_2(n) &= \frac{(1 + h/R_E) - \cos\xi}{(1 + h/R_E)\cos\xi - 1}
\end{aligned}$$

where

$$\begin{aligned}
\xi &= \frac{d}{2nR_E} \\
d &= \text{great circle distance between end points} \\
h &= \text{height of ionosphere} \\
n &= \text{number of ionospheric reflections in the path} \\
R_E &= \text{Radius of earth, } 6370 \times 10^3 \text{ metres}
\end{aligned} \tag{13.1}$$

This formula is valid up to a caustic limit where the factor $\alpha_2(n)$ has a pole at a great circle distance distance given by

$$d = 2nR_E \cos^{-1}\frac{1}{1 + h/R_E} \tag{13.2}$$

at which point the downwards propagating ray meets the ground at a tangent. This occurs at approximately 2000km for the single hop ($n = 1$) ray with $h = 80 \times 10^3$.

14 Hertzian Dipole

At VLF, a transmitting antenna approximates a vertical Hertzian dipole constituting a point source of TM waves. It consists of two vertically separated charge reservoirs of $\pm q$ separated by a distance l and connected by a uniform current I oscillating with angular frequency ω. It is characterised entirely by the equation

$$\begin{aligned}
Il &= -j\omega ql \\
&\text{where} \\
Il &= \text{current dipole moment} \\
ql &= \text{electric dipole moment} \\
q &= CV \\
C &= \text{antenna capacitance} \\
l &= \text{length of dipole} \\
I &= \text{antenna (peak) current} \\
V &= \text{antenna (peak) voltage}
\end{aligned} \tag{14.1}$$

The radiated far field of this source at range r along an angle ϕ to the dipole axis is given by

$$\begin{aligned}
E_\parallel &= -j\omega\mu Il\frac{e^{-j\omega r/c}}{4\pi r}\sin\phi \\
H_\perp &= E_\parallel/Z_0
\end{aligned} \tag{14.2}$$

If the dipole is at ground level with the earth forming one electrode, the radiation pattern is modified by the ground reflection coefficient $\Gamma_\parallel(\beta)$ described in section 8. The far field described by equation 14.3 must be multiplied by the factor $(1 + \Gamma_\parallel(\beta))$. Below the Brewster angle, $\Gamma_\parallel$ tends to -1 and the radiation is zero at zero elevation. However, at low elevations radiation also takes place via a Norton surface wave described in section 16. Ignoring the surface wave, the far field of a physical grounded vertical at range r along elevation angle β can be modelled by

$$\begin{aligned}
E_\parallel &= -j\omega\mu I_a h_a K_a \frac{e^{-j\omega r/c}}{4\pi r}(1 + \Gamma_\parallel(\beta))\cos\beta \\
&= -\omega^2\mu C_a V_a h_a K_a \frac{e^{-j\omega r/c}}{4\pi r}(1 + \Gamma_\parallel(\beta))\cos\beta \\
H_\perp &= E_\parallel/Z_0 \\
E_\perp &= H_\parallel = 0
\end{aligned}$$

where

$$\begin{aligned}
I_a &= \text{antenna current (peak)} \\
V_a &= \text{antenna voltage (peak)} \\
C_a &= \text{antenna capacitance} \\
h_a &= \text{antenna overall height}
\end{aligned} \tag{14.3}$$

The factor K_a is required to allow for the average current distribution, or equivalently, the average charge separation, or alternatively, an effective height coefficient. K_a will be 0.5 for a straight vertical wire, and closer to unity for a long horizontal wire.

The time averaged (RMS) power density is given by

$$S(r, \beta) = \frac{Z_0}{2}\left(\frac{\omega I_a h_a K_a}{4\pi r c}\right)^2 (1 + \Gamma_\parallel(\beta))^2 \cos^2\beta \tag{14.4}$$

Integrating the above over a sphere produces the total radiated power. For a unity ground reflection coefficient, the total power is

$$P_T = \frac{8\pi}{3} Z_0 \left(\frac{\omega I_a h_a K_a}{4\pi c}\right)^2 = \frac{I_a^2 R_T}{2} \tag{14.5}$$

where R_T is the radiation resistance of the antenna and the denominator 2 converts from peak current to RMS current.

The description of the far field, radiated power, and radiation resistance given above does not take account of radiation via the surface wave. This topic is covered in section 16.

15 Sky Ray Propagation Model

The received signal is the superposition of multiple rays. Each ray undergoes uniform expansion so that its amplitude is inversely proportional to the distance it travels.

A ray is labelled by the number of hops n. The ray n undergoes n ionospheric reflections and $n-1$ ground reflections. The ionospheric reflections occur at a zenith angle ϕ_n with reflection coefficients given in section 12. The ground reflections occur at elevation angles β_n with reflection coefficients defined in section 8. Each ray is also subject to the convergence coefficient described in section 13. The signal incident at the receiver from ray n is given by

$$\begin{bmatrix} E_{\parallel}^{(n)} \\ E_{\perp}^{(n)} \end{bmatrix} = \left([S]\,[T] \right)^{n-1} [S]\,\alpha(n) \frac{e^{-j\omega R_n/c}}{4\pi R_n} D \begin{bmatrix} 1 \\ 0 \end{bmatrix}$$

where

$$\begin{aligned} [S] &= \begin{bmatrix} {}_{\parallel}\Gamma_{\parallel}(\phi_n) & {}_{\perp}\Gamma_{\parallel}(\phi_n) \\ {}_{\parallel}\Gamma_{\perp}(\phi_n) & {}_{\perp}\Gamma_{\perp}(\phi_n) \end{bmatrix} \\ [T] &= \begin{bmatrix} \Gamma_{\parallel}(\beta_n) & 0 \\ 0 & \Gamma_{\perp}(\beta_n) \end{bmatrix} \\ D &= -j\omega\mu I_a h_a K_a (1+\Gamma_{\parallel}(\beta))\cos\beta \\ \phi_n &= \tan^{-1} \frac{R_E \sin\xi}{h + R_E(1-\cos\xi)} \\ \beta_n &= \pi/2 - \phi_n - \xi \\ \xi &= \frac{d}{2nR_E} \end{aligned} \tag{15.1}$$

A corresponding equation is satisfied by the magnetic field components. The components $E_{\parallel}^{(n)}$ and $E_{\perp}^{(n)}$ are respectively the TM and TE electric field strengths incident at the receiver site, not including the ground effects at the receiver. $\alpha(n)$ is the convergence coefficient for ray n given by equation 13.1 and R_n is the total path length of ray n given by

$$R_n = 2nR_E \frac{\sin\xi}{\sin\phi_n} \tag{15.2}$$

Equation 15.1 assumes uniform ground and ionosphere properties along the entire path, for simplicity of presentation. For numeric calculations it is straightforward to calculate the reflection matrices independently for each encounter with ground and ionosphere in order to take account of varying path properties such as land/sea, day/night, and path orientation with respect to the earth's magnetic field.

The total field incident at the receiver is the vector sum of the incident rays. The composite signal is an elliptically polarised wave as described in section 1. From equations 2.1 to 2.3, the fields to which the loops and vertical antenna respond are

$$\begin{aligned} H_{ns} &= \sum_n \left\{ H_{\perp}^{(n)} \cos\theta_s - H_{\parallel}^{(n)} \sin\beta_n \sin\theta_s \right\} \\ &= \sum_n \frac{1}{Z_0} \left\{ E_{\parallel}^{(n)} \cos\theta_s - E_{\perp}^{(n)} \sin\beta_n \sin\theta_s \right\} \\ H_{ew} &= \sum_n \left\{ H_{\perp}^{(n)} \sin\theta_s + H_{\parallel}^{(n)} \sin\beta_n \cos\theta_s \right\} \\ &= \sum_n \frac{1}{Z_0} \left\{ E_{\parallel}^{(n)} \sin\theta_s + E_{\perp}^{(n)} \sin\beta_n \cos\theta_s \right\} \\ E_v &= \sum_n E_{\parallel}^{(n)} \cos\beta_n \end{aligned} \tag{15.3}$$

where

θ_s = arrival azimuth of the rays

Typically, the sum must include rays up to $n = 10$ or $n = 20$ before further contributions are negligible at about the 1 percent level.

The azimuth θ and elevation β of the composite signal are then given by one of the direction finding methods described earlier. When using Tsuruda and Hayashi direction finding method described in section 5, there is no polarisation error and the result gives the true azimuth of the composite signal. Typically, this differs from the ray azimuth θ_s, and the difference is the multi-path error. When using the Poynting method of direction finding, there is also a polarisation error. In practice, the polarisation error and multipath error tend to cancel each other out and the Poynting method often produces the most reliable estimate of the actual source azimuth θ_s.

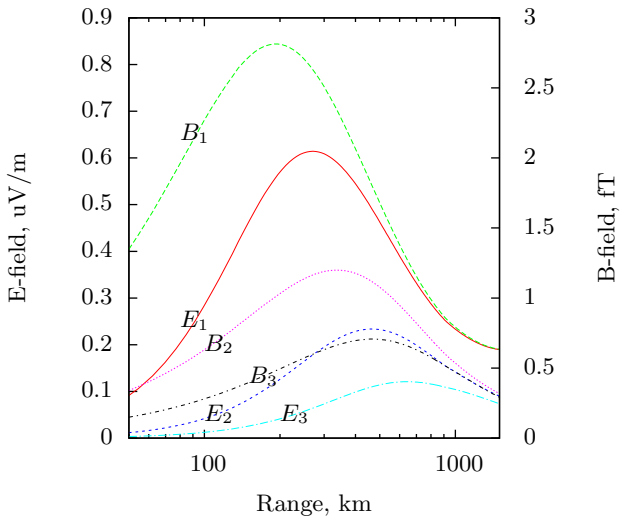

Figure 15.1: Vertical E-field and horizontal B-field components for the first three hops. Transmit power is 1mW at 6kHz

Figure 15.1 illustrates the amplitude of the first three hops of a signal at 6kHz, with the composite of the first 12 sky waves shown in figure 15.2. The vertical scales are commensurate at the free space impedance of 377 ohms, to which all the signals converge at long range. At short range the impedance appears lower due to the high elevation incidence of the signal.

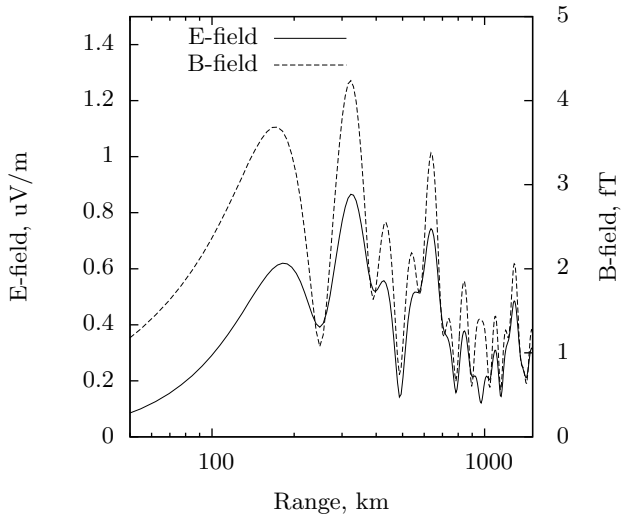

Figure 15.2: Vertical E-field and horizontal B-field components of the composite of 1-hop to 12-hop sky waves. Transmit power is 1mW at 6kHz

Ray modelling is effective up to a range approaching the caustic limit of the 1-hop ray. Beyond this range it is necessary to allow for surface diffraction, or to switch to waveguide mode modelling.

16 Ground Wave Propagation Model

The vertical E-field due to a vertical current element was given by equation 14.3 which takes account of the ground beneath the transmitter by including a coefficient of $1 + \Gamma_{\parallel}(\beta)$. At VLF, with β above a degree or so, $\Gamma_{\parallel}$ is close to $+1$. However, as the elevation reduces through the Brewster angle, the reflection coefficient phase rotates π degrees and the reflection coefficient tends to -1 as zero elevation is approached, causing the direct ray and ground reflected ray to cancel. Below the Brewster angle, another mode of radiation takes place - the Norton surface wave, with vertical E-field amplitude at ground range r given by,

$$E_{gv} = -j\omega\mu I_a h_a K_a \frac{e^{-j\omega r/c}}{4\pi r}(1 - \Gamma_{\parallel}(\beta))\frac{\tilde{n}^2 - 1}{\tilde{n}^2} W \quad (16.1)$$

where $\tilde{n}$ is the complex refractive index of the ground and W is a complex coefficient described below. This represents a wave diffracted along the ground surface, although it is not a true surface wave because the amplitude decays with $1/r$ rather than the $1/\sqrt{r}$ of a wave confined to the surface (a Zenneck wave). There is also a smaller horizontal radial E-field component, pointing away from the source, with amplitude

$$E_{gr} = \frac{E_{gv}}{\sqrt{\tilde{n}^2 - 1}} \quad (16.2)$$

For a flat earth, W is given by

$$\begin{aligned} W &= F(\Omega) \\ &= 1 - je^{-\Omega}\,\mathrm{erfc}\left(j\sqrt{\Omega}\right)\sqrt{\pi\Omega} \\ \Omega &= -j\frac{\omega}{c}\frac{\tilde{n}^2 - 1}{2\tilde{n}^4} r \end{aligned} \quad (16.3)$$

in which erfc() is the complimentary error function with complex argument. For a spherical earth, the coefficient W has a polynomial expansion

$$\begin{aligned} W &= F(\Omega) - \frac{\delta^3}{2}W_1 + \delta^6 W_2 + \ldots \\ W_1 &= 1 - j\sqrt{\pi\Omega} - (1 + 2\Omega)F(\Omega) \\ W_2 &= 1 - j(1 - \Omega)\sqrt{\pi\Omega} - 2\Omega + \frac{5\Omega^2}{6} + \left[\frac{\Omega^2}{2} - 1\right]F(\Omega) \\ \delta^3 &= -\frac{1}{2q^3} \\ q &= -j\frac{\sqrt{\tilde{n}^2 - 1}}{\tilde{n}^2}\left(\frac{\omega R_E}{2c}\right)^{1/3} \end{aligned} \quad (16.4)$$

The ground wave is significant at VLF out to a range of several hundred km, as illustrated in figure 16.1

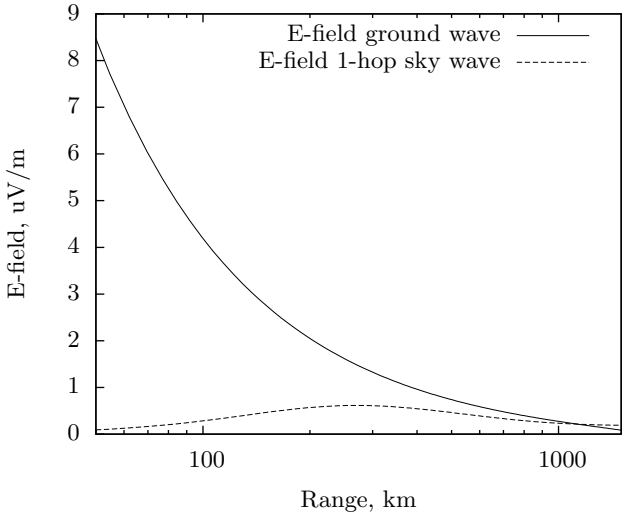

Figure 16.1: Vertical E-field and horizontal B-field components of the ground wave. The 1-hop sky wave is shown for comparison. Transmit power is 1mW at 6kHz

17 Loop Receiver Calibration

Consider a loop antenna with impedance Z_a composed of the reactance of the loop inductance L_a in series with the AC resistance R_a of the loop. Let the loop area be A and number of turns be N. We can safely neglect loop capacitance and radiation resistance.

The voltage induced in the loop by an incident flux B tesla passing through the loop will be

$$V_a = j\omega NAB \quad (17.1)$$

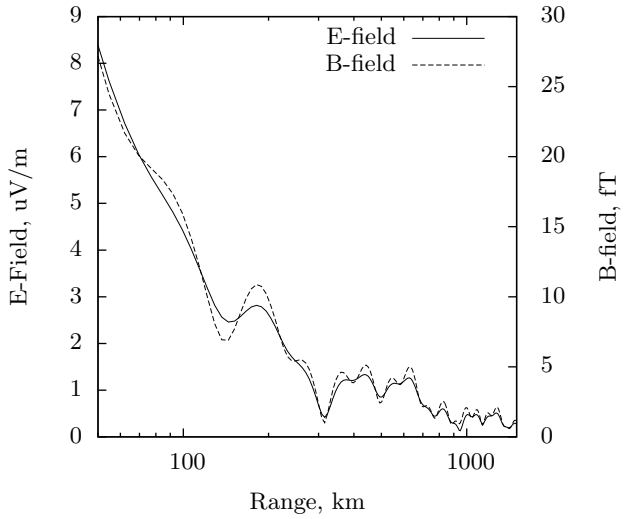

Figure 16.2: Vertical E-field and horizontal B-field components of the received signal. Ground and up to 12-hop sky waves combined. Transmit power is 1mW at 6kHz

and if a low-impedance receiver front end of input resistance R_r is in series with the loop, the current flowing in the loop and through the receiver's input will be

$$I_a = \frac{j\omega NAB}{R_r + R_a + j\omega L_a} \tag{17.2}$$

Now consider a calibration current I_{cal} injected from a test signal voltage V_{cal} delivered by a pad consisting of R_{cal} and C_{cal} in series. If R_{cal} is much greater than Z_a and R_r, the injected current is given by

$$I_{cal} = \frac{V_{cal}}{R_{cal} + \frac{1}{j\omega C_{cal}}} \tag{17.3}$$

A proportion of I_{cal} goes into the loop and the rest, I_{in} goes into the receiver, where I_{in} is given by

$$\begin{aligned} I_{in} &= I_{cal}\frac{Z_a}{R_r + Z_a} \\ &= \frac{V_{cal}}{R_{cal} + \frac{1}{j\omega C_{cal}}} \frac{R_a + j\omega L_a}{R_r + R_a + j\omega L_a} \end{aligned} \tag{17.4}$$

and we can equate this with the current into the receiver from a flux B given by equation 17.2,

$$\frac{j\omega NAB}{R_r + R_a + j\omega L_a} = \frac{V_{cal}}{R_{cal} + \frac{1}{j\omega C_{cal}}} \frac{R_a + j\omega L_a}{R_r + R_a + j\omega L_a} \tag{17.5}$$

If we choose C_{cal} so that

$$C_{cal} = \frac{L_a}{R_a R_{cal}} \tag{17.6}$$

then we find that equation 17.5 reduces to

$$V_{cal} = \frac{NAR_{cal}}{L_a} B \tag{17.7}$$

The quantities N, A, and L_a can be measured accurately, R_{cal} can be selected accurately, and C_{cal} and V_{cal} can be adjusted to reasonably good accuracy. The calibration is independent of the receiever's input resistance, so long as it is small compared to R_{cal}.

18 Simple Propagation Model

A simple propagation model for VLF assumes the radiated signal is trapped between the two spherical shells of the Earth-Ionosphere cavity, thus giving approximately a $1/\sqrt{r}$ field strength dependence on range r. Combining with an exponential decay factor to allow for average losses, we have,

$$E = \frac{300}{h} e^{-r/a} \sqrt{\frac{P_T \lambda}{R_E \sin(r/R_E)}}$$

where

E = field strength, volts/metre
r = great circle range, metres
a = attenuation factor,
$= 2.9 \times 10^6$(day),4.3×10^6(night)
P_T = effective radiated power, watts
h = D-region height, metres, 70×10^3 day, 95×10^3 night
R_E = Radius of earth, 6370×10^3 metres

(18.1)

19 Sferic Simulation

It is often useful to simulate a typical lightning sferic for the purpose of testing receiver and signal processing software. A commonly used method assumes that most of the energy of the lightning stroke is radiated from the lower few km of the lightning path, approximating a vertical Hertzian dipole so that all frequency components are radiated in phase. The sharp pulse of the discharge is then modeled by a sum of many cosines, all with zero phase. Each term of the sum is then multiplied by an amplitude weighting and a delay factor.

The field strength waveform at a distance r metres can be synthesized with a sum such as

$$V(t) = \sum A(\omega) cos\left(\omega\left(t - \frac{r}{v_p(\omega)}\right)\right) \tag{19.1}$$

where t is the time elapsed since the lightning discharge, and $v_p(\omega)$ is the phase velocity in the Earth-ionosphere cavity at the frequency ω. $v_p(\omega)$ is given by

$$v_p(\omega) = \frac{c}{\sqrt{1 - \omega_0^2/\omega^2}} \tag{19.2}$$

in which ω_0 is the cut-off frequency, typically 1700 Hz.

The sum over ω in 19.1 is usually taken from ω_0 up to the maximum frequency of interest. The amplitude coefficient $A(\omega)$ is chosen to represent the typical spectrum of a distant sferic. A simple example is

$$A(\omega) = \cos^2\left(\pi \frac{\omega - \omega_a}{2\omega_r}\right) \tag{19.3}$$

where ω_a is the angular frequency of the spectral peak and ω_r sets the spectral half-width. Then the sum in 19.1 is taken from ω_0 to $2\omega_r$.

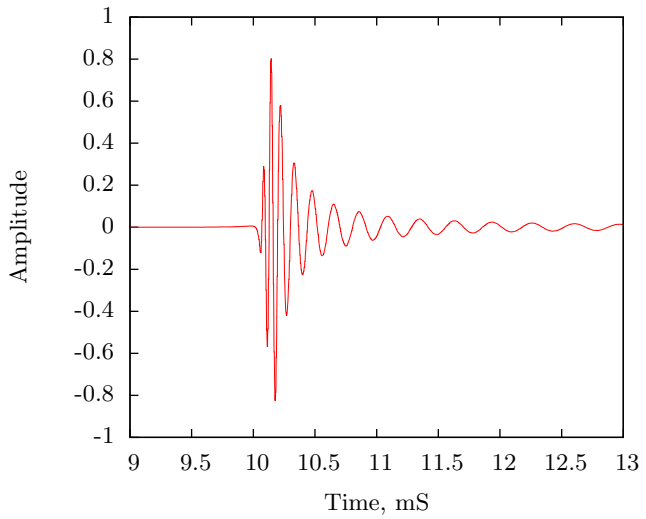

Figure 19.1: Synthetic sferic at range 3000km

An example of a synthesized sferic waveform is given in figure 19.1.

20 n-vectors

The commonly used latitude and longitude representation of a position on the Earth's surface is problematic for calculation purposes due to the mathematical singularities at the poles and the longitude discontinuity.

An alternative position representation which avoids these problems is the n-vector in which a position is represented by an outward pointing (vertical) unit 3-vector. Calculations involving positions, distances, and bearings on spherical or ellipsoidal Earth are considerably simplified when implemented with n-vectors.

n-vectors are usually expressed with respect to an Earth-centered cartesian coordinate basis. For example a point P with latitude λ and longitude μ can be represented by the n-vector

$$\hat{P} = \begin{bmatrix} P_x \\ P_y \\ P_z \end{bmatrix} = \begin{bmatrix} \cos(\lambda)\cos(\mu) \\ \cos(\lambda)\sin(\mu) \\ \sin(\mu) \end{bmatrix} \tag{20.1}$$

The north pole in this representation is

$$\hat{N} = \begin{bmatrix} 0 \\ 0 \\ 1 \end{bmatrix} \tag{20.2}$$

The conversion back to latitude and longitude is given by

$$\begin{aligned} \lambda &= \text{atan2}(P_z, \sqrt{P_x^2 + P_y^2}) \\ \mu &= \text{atan2}(P_y, P_x) \end{aligned} \tag{20.3}$$

Note that while there are no singularities in n-vector calculations, a singularity may occur when transforming back to latitude and longitude.

Directions are represented as unit 3-vectors using the same cartesian basis. For example, the northwards and eastwards directions from a n-vector point $\hat{P}$ are given by

$$\begin{aligned} \text{eastwards} &= \text{unit}(\hat{N} \times \hat{P}) \\ \text{northwards} &= \text{unit}(\hat{P} \times \hat{N} \times \hat{P}) \end{aligned} \tag{20.4}$$

where

$$\text{unit}(\hat{A}) = \frac{\hat{A}}{|\hat{A}|} \tag{20.5}$$

The great circle distance between two points represented by n-vectors $\hat{A}$ and $\hat{B}$ is given by

$$d = R_e \,\text{atan2}(|\hat{A} \times \hat{B}|, \hat{A} \cdot \hat{B}) \tag{20.6}$$

where R_e is the Earth radius.

The bearing of a forepoint $\hat{f}$ from a standpoint $\hat{s}$ is given by

$$\begin{aligned} \hat{x_1} &= \text{unit}(\hat{N} \times \hat{s}) \\ \hat{x_2} &= \text{unit}(\hat{f} \times \hat{s}) \\ \theta &= -\hat{s} \cdot \text{unit}(\hat{x_1} \times \hat{x_2})\, \text{atan2}(|\hat{x_1} \times \hat{x_2}|, \hat{x_1} \cdot \hat{x_2}) \end{aligned} \tag{20.7}$$

The forepoint $\hat{f}$ reached by travelling a distance d along a great circle with initial bearing θ from standpoint $\hat{s}$ is given by

$$\begin{aligned} D &= \text{unit}(\hat{s} \times \hat{N} \times \hat{s})\cos(\theta) + \text{unit}(\hat{N} \times \hat{s})\sin(\theta) \\ \hat{f} &= \hat{s}\cos\left(\frac{d}{R_e}\right) + D\sin\left(\frac{d}{R_e}\right) \end{aligned} \tag{20.8}$$

Averaging of a set of positions $\hat{A}_k$ is simply the normalised sum of the n-vectors,

$$\text{average position} = \text{unit}\left(\sum_k \hat{A}_k\right) \tag{20.9}$$

The point midway between two points $\hat{A}$ and $\hat{B}$ is just the normalised sum of the two vectors,

$$\text{midpoint} = \text{unit}(\hat{A} + \hat{B}) \tag{20.10}$$

and similarly, the point $\hat{C}$ at a fraction r of the way from $\hat{A}$ to $\hat{B}$ is

$$\hat{C} = \text{unit}(\hat{A}(1-r) + \hat{B}r) \tag{20.11}$$

The great circle joining two points $\hat{A}$ and $\hat{B}$ is represented by their normalised cross product,

$$\hat{c} = \text{unit}\left(\hat{A} \times \hat{B}\right) \tag{20.12}$$

and the two antipodal intersection points of great circles $\hat{c_1}$ and $\hat{c_2}$ are given by

$$\begin{aligned} \hat{P_1} &= \text{unit}\,(\hat{c_1} \times \hat{c_2}) \\ \hat{P_2} &= \text{unit}\,(\hat{c_2} \times \hat{c_1}) \\ &= -\,\text{unit}\,(\hat{c_1} \times \hat{c_2}) \end{aligned} \tag{20.13}$$